ARTICLE

JP1, a polypeptide specifically targeting integrin αVβ3, ameliorates choroidal neovascularization and diabetic retinopathy in mice

Zhan Xie[1], Xin-jing Wu[1], Rui-wen Cheng[1], Jia-hua Cui[2], Song-tao Yuan[1], Jian-wei Zhou[2] and Qing-huai Liu[1]

Anti-vascular endothelial growth factor (VEGF) drugs have revolutionized the treatment of neovascular eye diseases, but responses are incomplete in some patients. Recent evidence shows that integrins are involved in the pathogenesis of neovascular age-related macular degeneration and diabetic retinopathy. JP1, derived from an optimized seven-amino-acid fragment of JWA protein, is a polypeptide specifically targeting integrin αVβ3. In this study we evaluated the efficacy of JP1 on laser-induced choroidal neovascularization (CNV) and retinal vascular leakage. CNV mice received a single intravitreal (IVT) injection of JP1 (10, 20, 40 µg) or ranibizumab (RBZ, 10 µg). We showed that JP1 injection dose-dependently inhibited laser-induced CNV; the effect of RBZ was comparable to that of 20 µg JP1; a combined IVT injection of JP1 (20 µg) and RBZ (5 µg) exerted a synergistic effect on CNV. In the 3rd month after streptozotocin injection, diabetic mice receiving IVT injection of JP1 (40 µg) or RBZ (10 µg) once a week for 4 weeks showed significantly suppressed retinal vascular leakage. In both in vivo and in vitro experiments, JP1 counteracted oxidative stress and inflammation via inhibiting ROS/NF-κB signaling in microglial cells, and angiogenesis via modulating MEK1/2-SP1-integrin αVβ3 and TRIM25-SP1-MMP2 axes in vascular endothelial cells. In addition, intraperitoneal injection of JP1 (1, 5 or 10 mg) once every other day for 3 times also dose-dependently inhibited CNV. After intraperitoneal injection of FITC-labeled JP1 (FITC-JP1) or FITC in laser-induced CNV mice, the fluorescence intensity in the CNV lesion was markedly increased in FITC-JP1 group, compared with that in FITC group, confirming that JP1 could penetrate the blood-retinal barrier to target CNV lesion. We conclude that JP1 can be used to design novel CNV-targeting therapeutic agents that may replace current invasive intraocular injections.

Keywords: choroidal neovascularization; diabetic retinopathy; JP1; oxidative stress; inflammation; angiogenesis

INTRODUCTION

Severe and irreversible visual impairment may arise from an array of neovascular eye diseases, mainly including neovascular age-related macular degeneration (nAMD), diabetic retinopathy (DR), retinal vein obstruction retinopathy of prematurity, and neovascular glaucoma [1, 2]. Among them, nAMD remains a culprit for severe vision loss in the elderly [3], affecting 5% of those aged over 70. By 2050, the population affected by the disease is estimated to exceed 15 million worldwide [4].

Anti-vascular endothelial growth factor (VEGF) drugs have revolutionized the treatment of neovascular eye diseases. However, 67.4% of nAMD patients still suffer from persistent fluid exudation, and more than 60% from suboptimal vision recovery after two years of treatment [5–7]. Additionally, repeated anti-VEGF injections subject patients to a higher risk of developing complications, such as endophthalmitis, retinal pigment epithelium atrophy, and tears [8–11]. There is an urgent need to overcome the limitations of current anti-VEGF therapies [12].

As a family of transmembrane receptors mediating cell–cell and cell-extracellular matrix interactions [13], integrins are involved in the pathogenesis of multiple diseases, including cancer, nAMD, and DR [14]. In the blood vessels of nAMD patients, the levels of integrins αVβ3 and α5β1 increase significantly [15, 16]. Preclinical and early-phase clinical studies have detected the anti-integrin efficacy of drugs, such as risuteganib [17] and SF-0166 [18]. Therefore, targeting integrins may be employed to design primary therapy, adjunctive therapy (to anti-VEGF agents), or secondary therapy for refractory cases [14].

JWA gene is initially cloned through models of retinoic-acid-induced human bronchial epithelial cell differentiation [19]. JWA has an inhibitory effect on angiogenesis in gastric cancer [20] and melanoma [20]. JP1, derived from an optimized seven-amino-acid fragment of JWA protein, is a polypeptide specifically targeting integrin αVβ3. JP1 suppresses the growth and metastasis of melanoma [21], but whether and how it inhibits ocular neovascularization remain unknown. In the present study, we evaluated the efficacy of JP1 on laser-induced choroidal neovascularization (CNV) and retinal vascular leakage in the streptozotocin-induced diabetic mouse model, and explored its molecular mechanisms.

[1]Department of Ophthalmology, First Affiliated Hospital of Nanjing Medical University, Nanjing 210029, China and [2]Department of Molecular Cell Biology & Toxicology, Center for Global Health, School of Public Health, Nanjing Medical University, Nanjing 211166, China
Correspondence: Song-tao Yuan (songtaoyuan@njmu.edu.cn) or Jian-wei Zhou (jwzhou@njmu.edu.cn) or Qing-huai Liu (liuqh@njmu.edu.cn)
These authors contributed equally: Zhan Xie, Xin-jing Wu

898

MATERIALS AND METHODS

Peptide synthesis
JP1 was synthesized by GL Biochem (Shanghai, China) Ltd and Hybio Pharmaceutical Co., Ltd (Shenzhen, China). FITC-JP1 and FITC were synthesized by Zhejiang Peptides Biotech Co., Ltd (Hangzhou, China) with purities >98% confirmed by high-performance liquid chromatography. Freeze-dried peptide powder was stored at −20 ℃.

Mouse model of laser-induced CNV
C57BL/6 mice (aged 6–8 weeks, weighing 18–20 g) were maintained and bred at the Experimental Animal Center, Nanjing Medical University (Nanjing, China). Animal experiments were approved by the Animal Research Ethics Committee, Nanjing Medical University. Bruch's membrane was ruptured through laser photocoagulation to generate CNV as previously described [22]. After anesthesia, the pupils of the mouse were dilated with topical 5% tropicamide (Santen, Japan). Following mydriasis, the mouse was placed on a platform under a slit lamp, and its corneas were anesthetized with 0.5% proparacaine hydrochloride eye drops (Alcon, USA). Laser photocoagulation (532 nm laser, 250 mW, 100 ms duration, 50 μm spot) was performed bilaterally in each mouse. Laser burns were induced on spots at the 3, 6, 9, and 12 o'clock positions and about 1–2 PD around the optic disc. Only bubbled burns were included in our study. Burns showing hemorrhage or no bubble at the laser site were excluded. After laser modeling, all the mice were randomly divided into 9 groups ($n = 10$ per group). One group received single intravitreal (IVT) injection of 1 μL of 1× phosphate buffer saline (PBS) as controls. Five groups received IVT injections of 10, 20, 40 μg of JP1, 10 μg of ranibizumab (Lucentis, Gentech Inc., South San Francisco, CA, USA and Novartis), and 20 μg of JP1 combined with 5 μg of RBZ immediately after laser coagulation, respectively. The other three groups received intraperitoneal (i.p.) injections of 1, 5, or 10 mg of JP1 once every other day, respectively. The CNV was analyzed at d 7 after laser photocoagulation using fundus fluorescein angiography (FFA). FITC-dextran-labeled vessels on the flat-mounted choroid of model mice were also analyzed histologically.

Imaging of CNV
FFA was performed to analyze vascular leakage at baseline and d 7 after laser coagulation. The mouse was anesthetized and its pupils were dilated. The vascular leakage area and intensity were measured by FFA (sodium fluorescein 100 mg·mL^{-1}, Novartis, Switzerland). The leakage intensity at one CNV lesion was graded using ImageJ software (National Institutes of Health, Bethesda, MD, USA) by two masked researchers using the following criteria [23]: 0 (no leakage), faint hyperfluorescence or mottled fluorescence without leakage; 1 (questionable leakage), a hyperfluorescent area not increasing in size or intensity; 2A (leakage), a hyperfluorescent area increasing in intensity but not in size; and 2B (significant pathological leakage), a hyperfluorescent area increasing in both intensity and area.

FITC-dextran perfusion and measurements of CNV areas
Seven days after laser photocoagulation, the CNV mouse was subjected to general anesthesia and perfused with 0.2 mL of PBS containing 5 mg·mL^{-1} fluorescein-labeled dextran (FITC-dextran, average molecular weight 2×10^6; Sigma-Aldrich) through the left ventricle, as previously described [24]. Three minutes later, the CNV mouse was sacrificed; its eyes were isolated and fixed in 4% PFA for 1–2 h at room temperature. Four or five radial incisions were made to flatten the retinal pigment epithelial (RPE)-choroid-sclera complex on a glass slide, with the sclera facing down. CNV images were captured with a fluorescence microscope (BX53; Olympus, Japan) and the CNV area was measured using Image-Pro Plus 6.0 software (Media Cybernetics, Silver Spring, MD, USA) ($n = 24$ spots per group).

Histopathological analysis
The mouse was enucleated, and its eyes were fixed in 1% paraformaldehyde (PFA; Electron Microscopy Sciences, Hatfield, PA, USA) at 4 ℃ for 24 h. After fixation, the eyes were embedded in paraffin and serially sectioned (5 μm in thickness). Routine hematoxylin-eosin (HE) staining was performed on selected slides, and the serial sections were examined using a light microscope. From the sections of each eye, three largest spots were chosen to calculate the relative thickness of CNV lesions, and data from five eyes in each group were collected for the final evaluation.

Immunohistochemistry
For routine immunolocalization, the sections were dewaxed and rehydrated; incubated with 3% hydrogen peroxidase for 25 min and washed in PBS for 5 min; blocked with goat serum for 15 min; incubated with primary antibody overnight at 4 ℃, then with Goat Anti-Rabbit/Rat IgG antibody (Dako Denmark A/S, Denmark) for 30 min. Primary antibodies were as follows: anti-αV: (ab179475, 1:500, Abcam), anti-β3 (13166 s, 1:250, Cell Signaling Technology), anti-TNF-α (60291-1-Ig, 1:1000, Proteintech), anti-IL-6 (bs-0782R, 1:500, Bioss), and anti-VEGF (sc-53462, 1:500, Santa). The sections were subsequently incubated with horseradish peroxidase-conjugated streptavidin (Thermo Fisher Scientific China, Shanghai, China) for 30 min, then counterstained with hematoxylin for 2 min, and finally mounted in aqueous mounting medium. The results were examined using Scan Scope.

Immunofluorescence assay
The sections were washed with 1× PBS, then permeabilized with 0.3% Triton X-100. One hour later, the sections were incubated with blocking buffer (0.5% BSA and 0.1% Triton X-100 in PBS) for 1 h, and exposed to primary antibodies overnight at 4 ℃. Primary antibodies were as follows: anti-IBA1 (012-26723, 1:100, WAKO), anti-Nrf2 (16396-1-AP, 1:500, Proteintech), anti-TNF-α (ab183218, 1:100, Abcam), anti-IL-6 (bs-6309R, 1:100, Bioss), anti-CD31 (sc-376764, 1:100, Santa Cruz), Phospho-NF-κBp65 (Ser536, 1:1600, Cell Signaling Technology), anti-CD68 (ab283654,1:200, Abcam), anti-Occludin (27260-1-AP, 1:1600, Proteintech), anti-ZO-1 (21773-1-AP, 1:4000, Proteintech). Having been washed with PBS, the corresponding secondary antibodies (Alexa Fluor goat anti-mouse/rabbit with either 488 or 594 fluorescent probes, Life Technologies) were applied at room temperature for 2 h.

The immortalized mouse microglial line BV2 cells in passage 7 were used. The cells were seeded on coverslips, fixed with 4% paraformaldehyde for 15 min and permeabilized with 0.3% Triton X-100 for 30 min. Having been blocked in blocking buffer for 1 h at room temperature, BV2 cells were incubated with primary antibodies diluted in 5% fetal bovine serum (FBS) in PBS/0.3% Triton X-100 overnight at 4 ℃. Then, the glass coverslips were washed with PBS, followed by a 2-h incubation with fluorescein-conjugated secondary antibodies. Tissue sections containing cells were mounted with DAPI Fluoromount-G (0100-20, Southern Biotech). Fluorescence was visualized using a Leica microscope.

For choroidal flat mount immunostaining, RPE-choroid-sclera complexes were collected and fixed in 4% PFA for 15 min, blocked, and permeabilized. Choroids were stained with Griffonia Simplicifolia Lectin I (GSL I) isolectin B4, DyLight 594 (DL-1207-.5, 1:100, Vector), anti-IBA1(ab178846,1:200, Abcam), anti-CD31(ab24590, 1:200, Abcam) and anti-Integrin αVβ3 (sc-7312, 1:200, Santa) overnight at 4 ℃. RPE-choroid-sclerae were then washed and incubated with secondary antibody for 2 h at room temperature, washed and mounted in Antifade Mounting Medium with DAPI (P0131, Beyotime). The results were examined using Scan Scope.

RNA isolation and quantitative real-time PCR. Total RNA was extracted using TRNzol Universal (Tiangen). cDNA was synthesized with Evo M-MLV RT Premix for qPCR (Accurate Biotechnology).

Real-time PCR was performed using SYBR Green Premix Pro Taq HS qPCR Kit (Accurate Biotechnology) according to the manufacturer's instructions. Primer sequences (5′→3′) for PCR experiment were 5′-TTAAAAACCTGGATCGGAACCAA-3′ (forward) and 5′-GCATTAGCTTCAGATTTACGGGT-3′(reverse) for CCL2;5′-AGGTCCCTATGGTGCCAATGT-3′(forward) and 5′-CGGCAGGATTTTGAGGTCCA-3′(reverse) for CCL22;5′-TAGTCCTTCCTACCCCAATTTCC-3′ (forward) and 5′-TTGGTCCTTAGCCACTCCTTC-3′ (reverse) for IL-6; 5′-CCAAGTGCTGCCGTCATTTTC-3′ (forward) and 5′-GGCTCGCAGGGATGATTTCAA-3′ (reverse) for CXCL10; 5′-CAAGGCTGGTCCATGCTCC-3′ (forward) and 5′-TGCTATCACTTCCTTTCTGTTGC-3′ (reverse) for IL-8; 5′-GCTCTTACTGACTGGCATGAG-3′ (forward) and 5′-CGCAGCTCTAGGAGCATGTG-3′ (reverse) for IL-10; 5′-GGCTGTATTCCCCTCCATCG-3′ (forward) and 5′-CCAGTTGGTAACAATGCCATGT-3′ (reverse) for β-actin.

Biodistribution studies of FITC-JP1
One week after laser treatment, the mice were randomly divided into two groups (n = 10 per group), intraperitoneally injected with 100 μL of 5 mg FITC-labeled JP1 and 0.99 mg FITC (the mice in both groups were intraperitoneally injected with the same amount of FITC). FFA was used to measure the intensity of FITC in vivo (n = 5 per group). To evaluate the accumulation of FITC in CNV lesions, the mouse was euthanized at 1, 3, 8, 24, and 48 h after i.p. injection of FITC-JP1 or FITC. Afterward, the eyes were enucleated for fluorescence microscopy of flat-mounted choroids.

ROS detection in choroidal tissue sections
The eyeball was embedded in optimum cutting temperature compound (4583, SAKURA) and subjected to rapid freezing immediately after enucleation. Cryosections (10 μm in thickness) of the retinal pigment epithelium (RPE)-choroid were prepared. ROS was detected by staining with diluted fluoroprobe, 2′, 7′-dichlorodihydro-fluorescein diacetate DCFH-DA (HR7814, Biobrab). Fluorescence- microscopy was used to measure the ROS level in the retina-choroid section.

Measurement of MDA, SOD, and GPx
Glutathione peroxidase (GPx), maleicdialdehyde (MDA) and superoxide dismutase (SOD) in choroidal tissues were measured by kits according to the manufacturer's protocols (Beyotime Institute of Biotechnology, Jiangsu, China). Protein concentration was determined using a BCA protein assay kit (Beyotime Institute of Biotechnology, Jiangsu, China). All experiments were replicated for five times.

Intracellular ROS measurement
Intracellular ROS level was measured by the Reactive Oxygen Species assay kit (Beyotime Institute of Biotechnology, Jiangsu, China). Cells were incubated with DCFH-DA (Beyotime Institute of Biotechnology, Jiangsu, China) for 20 min at 37 °C. Having been washed with serum-free culture medium, the cells were examined under a fluorescence microscope.

Mouse model of STZ-induced retinal vascular leakage
C57BL/6 mice (male, aged 3–5 week) were rendered diabetic with five consecutive daily i.p. injections of streptozocin (STZ) (7.5 mg · mL^{-1}; S-0130, Sigma-Aldrich, St. Louis, MO, USA), freshly dissolved Na-Citrate (CAM) buffer (pH: 4.5–4.7; S4641, Sigma) at 50 mg · kg^{-1} [25]. Non-diabetic mice received five consecutive injections of CAM buffer alone. One week later, a blood glucose level ≥300 mg · dL^{-1} was considered as diabetic onset. Only the mice with consistent high glucose level for 3 weeks were used for subsequent experiments. Insulin was not used in diabetic groups. Blood glucose level was measured monthly to confirm diabetic status. Two months after diabetic onset, 10 age-matched non-diabetic mice were screened, in parallel with four groups of STZ-induced diabetic mice (10 mice receiving 1 μL of PBS, 10 mice receiving 1 μL of 40 μg JP1, 10 mice receiving 1 μL of 10 μg RBZ and 10 mice receiving 1 μL of 5 μg RBZ combined with 20 μg JP1, respectively). IVT injection was performed once a week for 4 weeks, the frequency of which was equal to that in human patients (3 initial monthly + pro re nata injections). The Evans blue (EB) assay was used to evaluate retinal vascular permeability. FITC-dextran was perfused to observe retinal vessels in diabetic and control groups at 4 weeks after initiation of IVT treatment.

Evans blue assay
Blood-retinal barrier breakdown (BRB) was quantified using the Evans blue assay as described previously with minor modifications [26]. The Evans blue (45 mg · kg^{-1}) was injected for over 10 s through the tail vein of the mouse. Then, the mouse was kept on a warm pad for 2 h. Afterward, 100 μL of blood was drawn and plasma Evans blue concentration was measured. The chest cavity was opened, and the mouse was perfused with citrate buffer (0.05 M, pH 3.5) for 2 min via the left ventricle at 37 °C to clear the dye from the vessel. Next, both eyes were enucleated and bisected along the equator. Retinae were dissected under a stereomicroscope and dried at 70 °C for 24 h. Evans blue dye conjugated with serum albumin in the retina was extracted by incubating each sample in 130 μL of formamide (Sigma) for 18 h at 70 °C. The extract was centrifuged at 65,000 r/min at 4 °C for 60 min. The blood samples were centrifuged at 12,000 rpm at 4 °C for 15 min, and diluted to 1/100 in formamide prior to spectrometric evaluation. To assess the Evans blue concentration, the absorbance in retinal extract and plasma samples was measured at 620 nm and in comparison with a standard curve. BRB was calculated using the following equation: Evans blue (μg)·Retina dry weight (g)$^{-1}$·Evans blue concentration (μg)$^{-1}$·Plasma (μL)·Circulation time (h)$^{-1}$. The results were expressed as microliters plasma × gram retina dry wt^{-1}· h^{-1}.

FITC-dextran-labeled flat-mounted retinas
Retinal neovascularization in the flat-mounted retinae was quantified as previously reported with minor modifications [22, 26]. First, 1 mL of 1× PBS containing 40 mg · mL^{-1} fluorescein isothiocyanate-dextran (average mol wt: 2×10^6, Sigma, St Louis, MO, USA) was perfused through the left ventricle of the anesthetized mouse. Five min later, the eyes were enucleated and fixed in 4% paraformaldehyde overnight. Following corneal excision, the retinae were removed under a stereomicroscope. The retinae were cut centripetally from the edge to the equator and then flat-mounted. The flat mounts were viewed by a fluorescence microscope and photographed. Using the Angio Tool image analysis software 10, the density of the capillary network in five parts of the retina of each eye was calculated [26].

Cell culture and treatment
Human umbilical vein endothelial cells (HUVECs) were purchased from Shanghai Institute of Biochemistry and Cell Biology, Chinese Academy of Sciences (Shanghai, China); the cells were cultured in RPMI-1640 (Thermo Scientific) supplemented with 10% fetal bovine serum (FBS; Gibco), 1% streptomycin and penicillin (Gibco) in a humidified incubator at 37 °C with 5% CO$_2$; and treated with VEGF (50 ng · mL^{-1}) in the presence or absence of JP1 at indicated doses (0, 50, 100, 200 μM) for 24 h.

The immortalized mouse microglia cell line BV2 was donated by Professor Han Feng from the Department of Clinical Pharmacology, School of Pharmacy, Nanjing Medical University. BV2 cells in passage 7 were maintained in DMEM/F12 (Biosharp) supplemented with 10% FBS, 1% penicillin/streptomycin and 1% GlutaMAX (Gibco). Then, the cells were treated with lipopolysaccharide (LPS) (1 μg · mL^{-1}) in the presence or absence of JP1 at indicated doses (0, 50, 100, 200 μM) for 24 h.

HUVECs tube formation assay
For tube formation assay, the 96-well plates were coated with 50 μL of Matrigel™ (BD Biosciences) and kept at 37 °C for 2 h. Then HUVECs suspended in 100 μL of conditioned medium were seeded into the precoated 96-well plates (1.2×10^4 per well). After incubation at 37 °C for 4 h, tubular structures formed in the Matrigel were captured in five randomly selected fields per sample under a microscope.

5-Ethynyl-20-deoxyuridine (EdU) assay
An Edu kit (Cell Light EdU DNA Imaging kit, RiboBio) was used to evaluate the proliferative ability of HUVECs according to the manufacturer's instructions. Images were obtained and analyzed with a microscope (Olympus, Tokyo, Japan). The ratio of 5-ethynyl-20-deoxyuridine (EdU)-stained cells (red fluorescence) to DAPI-stained cells (blue fluorescence) was used as an index of cell proliferation.

Transwell migration assay
HUVECs (2.5×10^5) were suspended in 250 μL of serum-free DMEM and seeded into the top chambers of 24-well Transwell plates (Corning Inc., Corning, NY). The bottom chambers of the Transwell plates were filled with 600 μL of DMEM containing 10% FBS. After 48 h, the bottom of each chamber insert was stained with methanol and 0.1% crystal violet, and the cells were imaged and counted using an Olympus IX70 inverted microscope (Tokyo, Japan).

Western blot analysis
Western blot analysis was performed as previously described [21]. Briefly, the cell samples were lysed in lysis buffer (50 mM Tris, pH 7.4; 150 mM NaCl; 1% NP-40; 0.5% sodium deoxycholate; 0.1% SDS; and the protease inhibitor, 1 mM PMSF), and the tissue samples were prepared in tissue protein extraction reagent (Thermo Fisher Scientific). Protein (40 μg) was extracted. The antibodies used were as follows: anti-CD31 (sc-376764, 1:100, Santa Cruz), anti-αV: (ab179475, 1:5000, Abcam), anti-β3 (4702s, 1:1000, Cell Signaling Technology), anti-MMP2 (18309-1-AP, 1:1000, Proteintech), anti-TRIM25 (12573-1-AP, 1:1000, Proteintech), anti-MEK1/2 (1:1000, Cell Signaling Technology), anti-p-MEK1/2 (Ser217/221, 1:1000, Cell Signaling), anti-SP1 (21962-1-AP, 1:1000, Proteintech), anti-VEGF (sc-53462, 1:200, Santa Cruz), anti-NF-κBp65 (66535-1-Ig, 1:1000, Proteintech), anti-p-NF-κBp65 (Ser536, 1:1000, Proteintech), anti-Occludin (27260-1-AP, 1:1000, Proteintech), anti-ZO-1 (21773-1-AP, 1:1000, Proteintech), anti-TNF-α (17590-1-AP, 1:1000, Proteintech), anti-IL-6 (bs-0782R, 1:1000, Bioss), anti-Nrf2 (16396-1-AP, 1:2000, Proteintech), anti-β-actin (AF0003, 1:1000, Beyotime), anti-GAPDH (AF5009, 1:1000, Beyotime), anti-Tubulin (AT819, 1:1000, Beyotime).

Statistical analysis
All data were presented as mean ± standard error of mean (SEM). Student's t test was performed for comparison between groups, and one-way ANOVA for comparison among three or more groups. Statistical significance was defined by a P value <0.05. Statistical analysis was performed with the GraphPad Prism v9.0 software (GraphPad Software, Inc., La Jolla, CA, USA).

RESULTS
IVT injection of JP1 ameliorates laser-induced CNV in mice
We first observed that IVT injection of JP1 inhibited laser-induced CNV in a dose-dependent manner (Fig. 1a). Laser induced significant vascular leakage in the control group, while high (40 μg/eye), medium (20 μg/eye) and low (10 μg/eye) doses of JP1 exerted therapeutic effects, as shown by means of FFA (Fig. 1b). In the JP1 groups, the percentages of CNV lesions with 0 and 1 leakage scores increased, but those with 2a and 2b leakage scores

decreased (Fig. 1c). Representative images of FITC-dextran-labeled CNV were captured (Fig. 1d). IVT injection of JP1 obviously reduced the size of laser-induced CNV area, compared to that in the control group (Fig. 1e). High-dose JP1 had a stronger inhibitory effect than RBZ, and the effect of RBZ was comparable to that of medium-dose JP1 (Fig. 1e). HE staining showed the thickening of CNV area after combined treatment with JP1 (20 μg) and RBZ (5 μg), suggesting the rapid regression of CNV (Fig. 1f, g). At 1 week after laser treatment, all three doses of JP1 potently inhibited CNV-induced vascular leakage in a dose-dependent manner (Fig. 1e, g). Interestingly, combined treatment with JP1 (20 μg) and RBZ (5 μg) exerted a synergistic effect on CNV, which was much stronger than that of JP1 or RBZ alone (Fig. 1e, g).

JP1 decreases the recruitment and activation of microglial cells in CNV lesions
Subretinal accumulation of microglia cells is closely associated with CNV formation in AMD specimens and AMD-relevant animal models [27]. To further explore the therapeutic effects of JP1 on the microglial cells of CNV mice, the choroidal flat mounts were stained with IBA1 (a microglial cell marker) and CD31 (a vascular endothelial cell marker) at d 7 following laser treatment. In response to laser injury, the microglia polarized towards the lesion and shielded the injured area with an accumulation of microglial extensions in PBS group, and JP1 reduced recruitment and activation of microglial cells in CNV lesions (Fig. 2a). The mice in the PBS group experienced a higher degree of infiltration of choroidal microglial cells, compared to those in the JP1 group (Fig. 2b). Prolonged tissue stress can prime microglia overly reactive and into a phenotype associated with the secretion of pro-inflammatory mediators, including chemokines and cytokines [28, 29]. Therefore, we detected the mRNA expression of several cytokines in RPE/Choroids at d 7 after laser treatment, particularly those previously reported associated with neovascularization [30, 31]. Chemokines CCL2, CCL22, CXCL10, IL-6, IL-8, and IL-10 were all significantly downregulated in the JP1-treated RPE/choroids (Fig. 2c–h).

JP1 attenuates oxidative stress and inflammation in microglial cells in the CNV model
Oxidative stress and inflammation are two pathological hallmarks contributing to AMD [32, 33]. To evaluate oxidative stress, we performed immunofluorescence staining to detect the generation of ROS in choroidal tissue sections (Fig. 3a). Compared with the control group, JP1 groups showed lower levels of ROS in the frozen sections of CNV lesions (Fig. 3a). Additionally, the levels of antioxidant enzymes (SOD and GPx) were increased significantly in choroidal tissues after JP1 treatment, while that of MDA was decreased significantly (Fig. 3b).

Previous studies have shown that JWA activates Nrf2 expression and inhibits ROS production, thus enhancing the resistance of neuronal cells to paraquat-induced toxicity [34]. In this study, double staining of laser-induced CNV lesions with IBA1 (green) and Nrf2 (red) showed that JP1 markedly reduced infiltration of IBA1-positive microglial cells and enhanced immunoreactivity to Nrf2 in choroidal tissue (Fig. 3c). Western blot analysis also showed significantly increased Nrf2 protein expression in choroidal tissue after JP1 treatment (Fig. 3d).

Oxidative stress induces inflammation during the development of AMD [35]. Considering the involvement of NF-κB signaling in ROS generation, we detected the anti-inflammatory effect of JP1 in microglia cells using a laser-induced CNV model and a BV2 mouse microglia cell line. Compared with that in the control group, the immunoreactivity to p-P65 was reduced in JP1 groups (Fig. 3e). Western blot analysis showed that JP1 suppressed the phosphorylation of P65 in choroidal tissues (Fig. 3f). Next, we detected the expression of two inflammation biomarkers (TNF-α and IL-6) in CNV lesions. The immunofluorescent staining
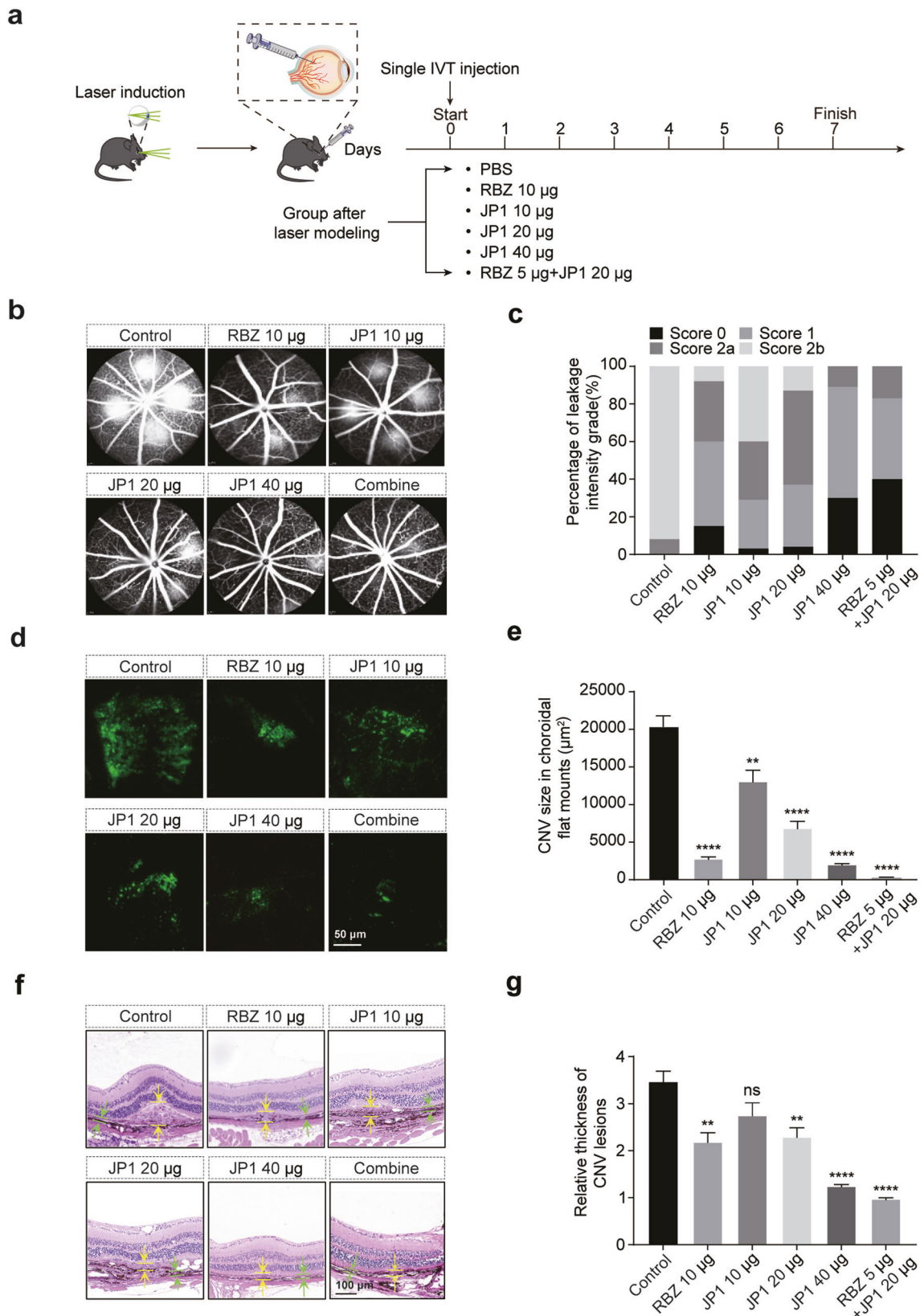
Fig. 1 JP1 suppressed and resolved CNV. a Schematic diagram of experimental procedures. **b** Representative FFA images of mice treated with PBS, JP1, and RBZ. **c** Percentages of CNV lesions graded according to leakage intensity. **d** Representative images of FITC-dextran-labeled blood vessels on a flat-mounted choroid, scale bar: 50 μm. **e** Quantitative analysis of fluorescent vessels by computerized analysis with ImageJ software. **f** HE staining of CNV lesions, scale bar: 100 μm. **g** Quantitative analysis of CNV lesion thickness. Data in **c**, **e**, and **g** were expressed as mean ± SEM. ns no difference from control; **P ≤ 0.01 vs control; ****P ≤ 0.0001 vs control. IVT intravitreal, RBZ Ranibizumab.
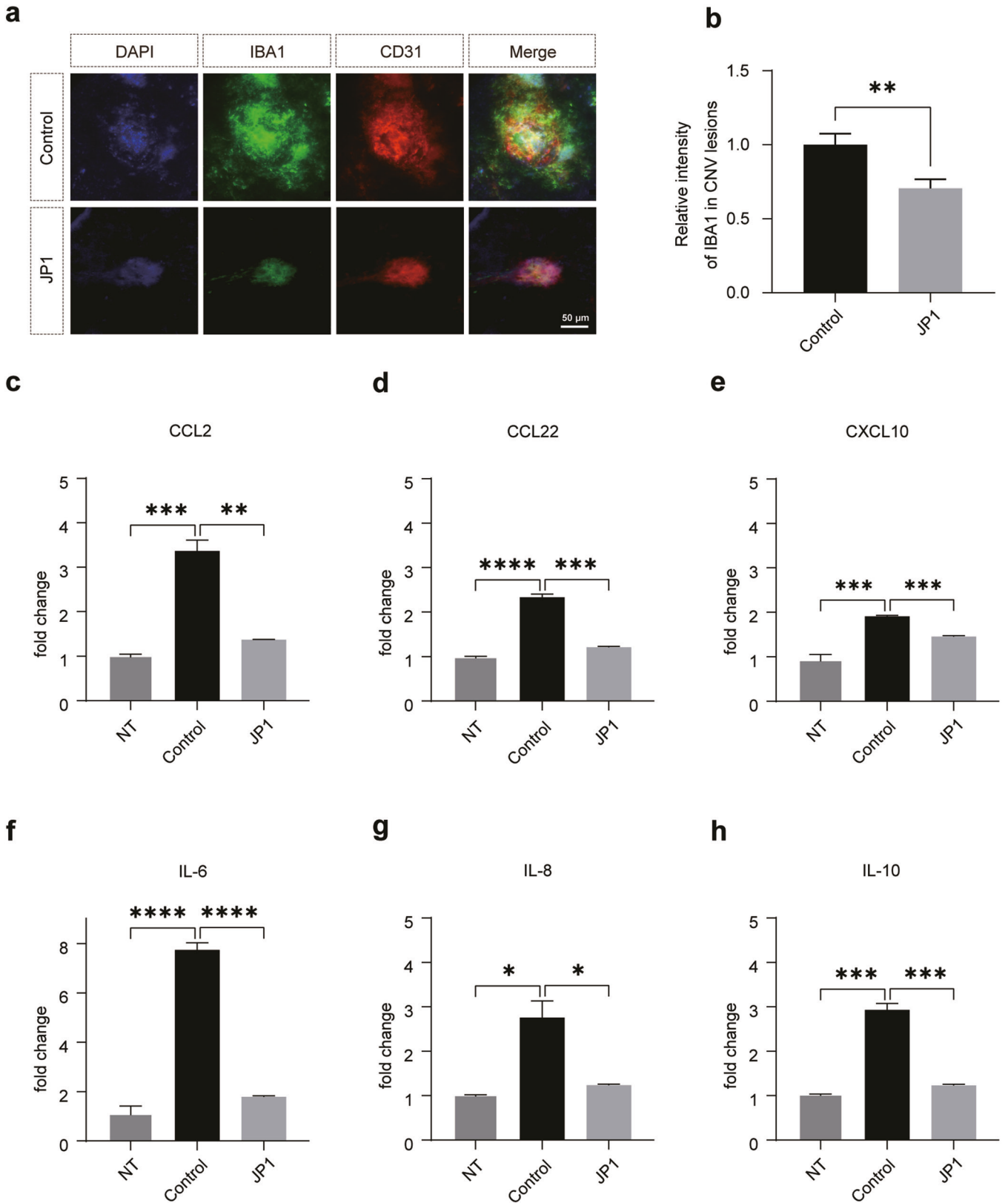
Fig. 2 **JP1 decreases microglials activation and infiltration into CNV areas, with downregulation of some chemokines. a** Representative images of CNV immunostaining. The samples were stained with DAPI (blue), IBA1(green) and CD31 (red) in CNV mice receiving IVT injection of 1 μL of PBS or JP1 40 μg at d 7 post-laser treatment. Scale bar: 50 μm. **b** Quantitative analysis of the intensity of IBA1 in CNV lesions ($n = 3$ mice per group). mRNA expression levels of chemokines CCL2 (**c**), CCL22 (**d**), CXCL10 (**e**), IL-6 (**f**), IL-8 (**g**), and IL-10 (**h**) in RPE/Choroids of non-treated and laser-treated CNV mice receiving IVT injection of 1 μL of PBS or JP1 40 μg ($n = 3$ mice per group). Data in **b–h** were expressed as mean ± SEM. *$P \leq 0.05$ vs control; **$P \leq 0.01$ vs control; ***$P \leq 0.001$ vs control; ****$P \leq 0.0001$ vs control. NT non-treated.

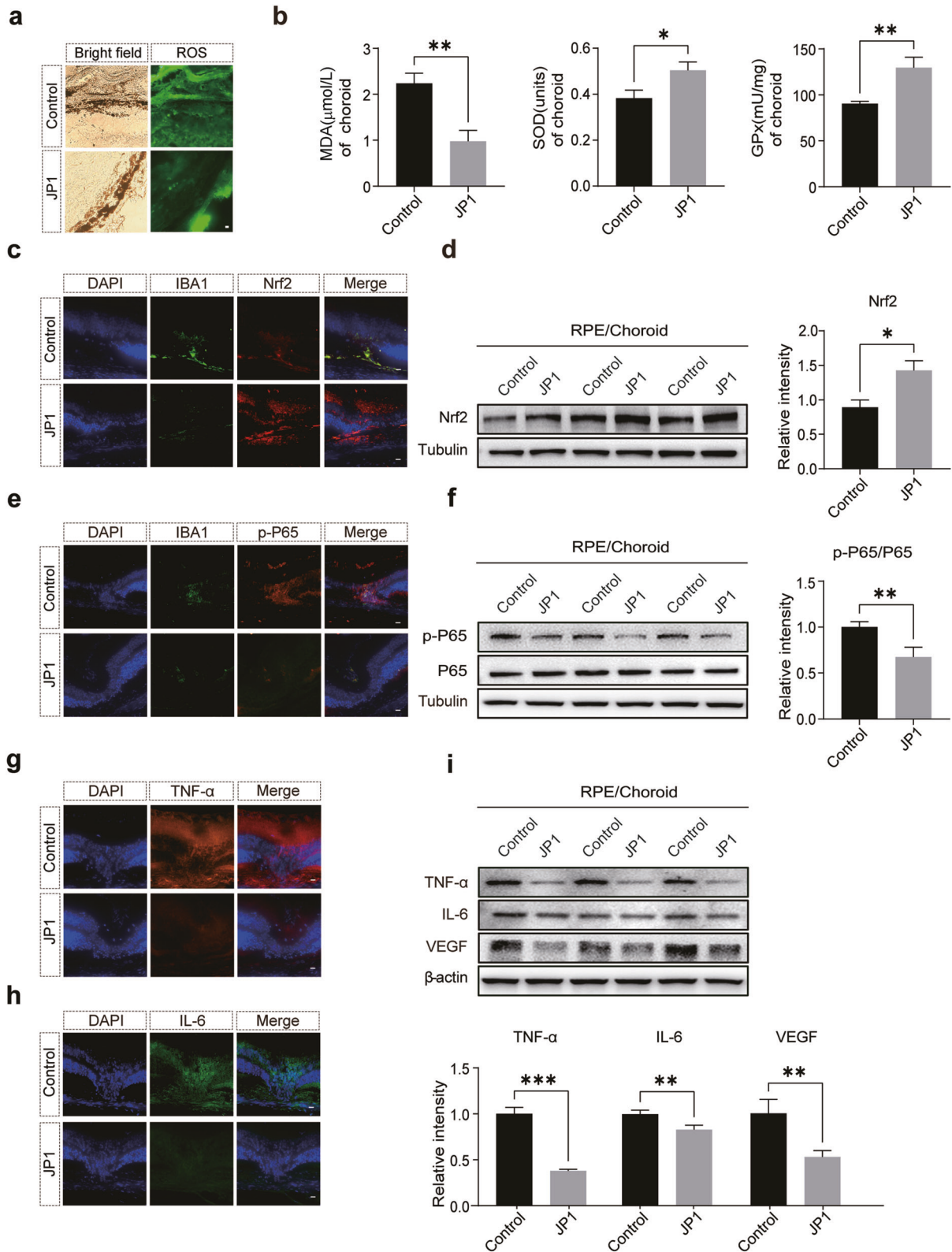**Fig. 3 JP1 attenuated oxidative stress and inflammation in microglial cells in the CNV models. a** Immunostaining of ROS in CNV lesions of mice receiving IVT injection of 1 μL of PBS or JP1 40 μg, scale bar: 10 μm. **b** Measurement of MDA, SOD, and GPx activities in RPE/choroidal tissue. **c** Immunofluorescent evaluation of IBA1 and Nrf2 in choroidal neovascular tissue of CNV lesions, scale bar: 10 μm. **d** Western blot analysis of Nrf2 in choroidal neovascular tissue of CNV lesions. **e** Immunofluorescent evaluation of IBA1 and p-P65 in choroidal neovascular tissue of CNV lesions, scale bar: 10 μm. **f** Western blot analysis of p-P65 and P65 of RPE/choroidal tissues; Immunofluorescent evaluation of TNF-α (**g**) and IL-6 (**h**) in choroidal neovascular tissue of CNV lesions, scale bar: 10 μm. **i** Western blot analysis of TNF-α, IL-6, and VEGF of RPE/choroidal tissues in PBS or JP1-treated CNV mice. Data in **b**, **d**, **f**, and **i** were expressed as mean ± SEM. *$P \leq 0.05$ vs control, **$P \leq 0.01$ vs control, ***$P \leq 0.001$ vs control.

904

(Fig. 3g, h) and Western blot (Fig. 3i) results showed that TNF-α and IL-6 expression was significantly downregulated in JP1-treated eye tissues, accompanied by decreased protein level of VEGF expression (Fig. 3i).

JP1 reduces LPS-induced oxidative stress and inflammation in BV2 cells

To confirm the mechanism underlying the counteractive effects of JP1 on oxidative stress and inflammation in microglial cells, mouse microglia BV2 cells were treated with LPS (1 μg·mL^{-1}) in the presence or absence of JP1 (0, 50, 100, 200 μM) for 24 h. CD68 staining was used to mark the active M1 microglial phenotype [36, 37]. We used a quantitative cell-based fluorescence assay for the measurement of ROS in BV2 cells (Fig. 4a). A 24-h treatment with LPS (1 μg·mL^{-1}) provoked a robust increase of ROS in microglial cells (Fig. 4a, b). ROS production was negatively correlated with JP1 level in BV2 cells (Fig. 4a, b). Additionally, immunofluorescent staining (Fig. 4c, d) and Western blot analysis (Fig. 4e) revealed that JP1 dose-dependently upregulated the level of Nrf2. Our findings were in line with those previously reported [34]. Next, we detected the anti-inflammatory potential of JP1 using LPS-treated BV2 cells. Notably, the immunofluorescence of stained CD68 increased significantly after LPS stimulation, while JP1 downregulated this increase, which indicated the inhibitory effect of JP1 on inflammatory response may be due to the suppression on M1 polarization (Fig. 4c, f). Immunofluorescent staining further showed upregulation by LPS and dose-dependent downregulation by JP1 on p-P65 and pro-inflammatory factors (TNF-α, IL-6, and iNOS) in BV2 cells (Fig. 4f–h). Western blot analysis confirmed that a 24-h treatment with LPS activated NF-κB pathway, accompanied by upregulation of inflammatory factors (VEGF, TNF-α, and IL-6), while JP1 suppressed the phosphorylation of P65 and reduced the levels of inflammatory factors effectively in a dose-dependent manner (Fig. 4i). These results confirmed that JP1 exerted potent counteractive effects on oxidative stress and inflammation in microglial cells by inhibiting the ROS/NF-κB signaling.

JP1 inhibits angiogenesis via modulating the MEK1/2/SP1/Integrin αVβ3 and TRIM25/SP1/MMP2 axes both in vivo and in vitro

JP1 is a functional polypeptide derived from the active fragment of JWA protein [21]. Thus, we hypothesized that JP1 inhibits CNV through a mechanism similar to that of JWA in countering tumorigenesis [21, 38, 39], and investigated it with in vivo and in vitro experiments.

JP1 has been reported to inhibit melanoma via modulating the MEK1/2/SP1/Integrin αVβ3 axis [21]. Therefore, we detected the expression of integrin αV and β3 in the tissue of CNV lesions. Immunohistochemical studies showed downregulation of integrin αV and β3 in JP1-treated tissue (Fig. 5a). Next, we detected the expression of MEK1/2, p-MEK1/2, integrins αV, β3, SP1, and CD31 in the choroidal tissue of CNV lesions by Western blot analysis. As shown in Fig. 5b, JP1 reduced the phosphorylation of MEK1/2 and SP1, accompanied by the downregulation of integrin αV, β3, and CD31 protein levels (Fig. 5b). In addition, previous studies have shown that JWA inhibits tumor angiogenesis in gastric cancer via modulating the TRIM25-SP1-MMP2 axis [20, 39]. Next, we detected that JP1 downregulated TRIM25 and MMP2 protein levels in the choroidal tissue of CNV lesions (Fig. 5c).

To further confirm the mechanism of JP1 in inhibiting angiogenesis, we performed transwell assay, EdU assay, tube formation assay, and Western blot analysis, respectively. HUVECs were incubated with VEGF (50 ng·mL^{-1}) in the presence or absence of different doses of JP1 (0, 50, 100, 200 μM) for 24 h. The results showed that JP1 dose-independently inhibited VEGF-induced tube formation (Fig. 5d, e), migration (Fig. 5f, g) and proliferation (Fig. 5h, i) of HUVECs. JP1 modulated the MEK1/2-SP1-Integrin αVβ3 and TRIM25-SP1-MMP2 axes in a dose-

dependent manner (Fig. 5j, k), which was in line with the results in vivo.

JP1 alleviates BRB disruption partly via modulating NF-κB activation in retinal microglial cells in the mouse STZ model

Inflammation is a main pathologic feature of DR [40, 41]. DR develops as inflammatory factors are released to activate NF-κB signaling pathway in microglial cells [42–49]. JWA gene protects neurons against dopamine neuronal degeneration via modulating the NF-κB signaling pathway [50]. We analyzed whether JP1 could alleviate BRB disruption in STZ-induced diabetic mice and modulate the NF-κB signaling pathway (Fig. 6a).

As shown by retinal flat mounts, a 3-month diabetes increased vascular leakage around the optic disk and peripheral retina, along with retinal vascular tortuosity, and shrunk non-perfused areas in model mice (Fig. 6b). Vascular density decreased significantly in PBS-treated eyes, but not in RBZ- or JP1-treated groups (Fig. 6c). Compared to 40 μg of JP1 or 10 μg of RBZ alone, their combination (20 μg of JP1 or 5 μg of RBZ) was superior in regulating vessel density (Fig. 6c). Furthermore, the permeability remained higher in PBS-treated group, but not in the other four JP1-treated groups (Fig. 6d). These results verified the evident efficacy of JP1 in inhibiting vascular leakage in the diabetic mouse model.

To further explore how JP1 alleviates BRB disruption in the condition of diabetic retinopathy, we evaluated the level of inflammation and the integrity of tight junction proteins in the retina. Compared with the PBS-treated group, the immunoreactivity to p-P65 and IBA1 demonstrated reduction in JP1-treated groups (Fig. 6e). Immunohistochemical staining also revealed downregulation of TNF-α, IL-6 and VEGF in the retinal tissue of diabetic mice injected with JP1 (Fig. 6f). Western blot analysis further confirmed that JP1 repressed NF-κB signaling pathway and inflammation factors (VEGF, TNF-α and IL-6) (Fig. 6g). In addition, immunohistochemistry (Fig. 6h), immunofluorescence (Fig. 6i) and Western blot analysis (Fig. 6j) revealed that JP1 alleviated the damage on tight junction proteins (Occludin and ZO-1) in the retinae of diabetic mice.

Intraperitoneal injection of JP1 reduces CNV leakage and area

Integrin αVβ3 is overexpressed in tumor cells and activated endothelial cells [51]. Integrins recognizing RGD peptide have been particularly investigated as therapeutic targets of tumors [41, 52]. JP1 is designed as a peptide-linked RGD motif targeting integrin αVβ3. We explored the potential of JP1 (i.p.) in inhibiting CNV in the laser-induced mouse model (Fig. 7a). Vascular leakage grades (Fig. 7b), mean CNV areas (Fig. 7c) and relative thicknesses of CNV lesions (Fig. 7d) indicated that JP1 potentially inhibited CNV in a dose-dependent manner. Staining of Integrin αVβ3 (green) and IB4 (red) was performed on choroidal flat mounts at 7 d following laser treatment (Fig. 7e). The immunoreactivity to Integrin αVβ3 and IB4 was reduced in JP1 i.p. groups dose-dependently (Fig. 7e).

FFA and fluorescence microscopy were conducted after i.p. injection of FITC-JP1 and FITC at indicated time points in the laser-induced CNV mouse model (Fig. 8a). Fluorescence in the CNV lesions was still visible at 24 h in the FITC-JP1 group, but not in the FITC group (Fig. 8b). Fluorescence intensity in eyes was higher in the FITC-JP1 group than in the FITC group (Fig. 8c). Microscopy of flat-mounted retinal choroid confirmed that JP1 enhanced FITC accumulation in CNV lesions (Fig. 8d, e). The above evidences suggested that i.p. JP1 injection reduced CNV leakage and area.

DISCUSSION

In the present study, we found that JP1 relieved CNV via modulating ROS/NF-κB signaling in microglial cells and SP1-Integrin αVβ3/MMP2 signaling in vascular endothelial cells. Our
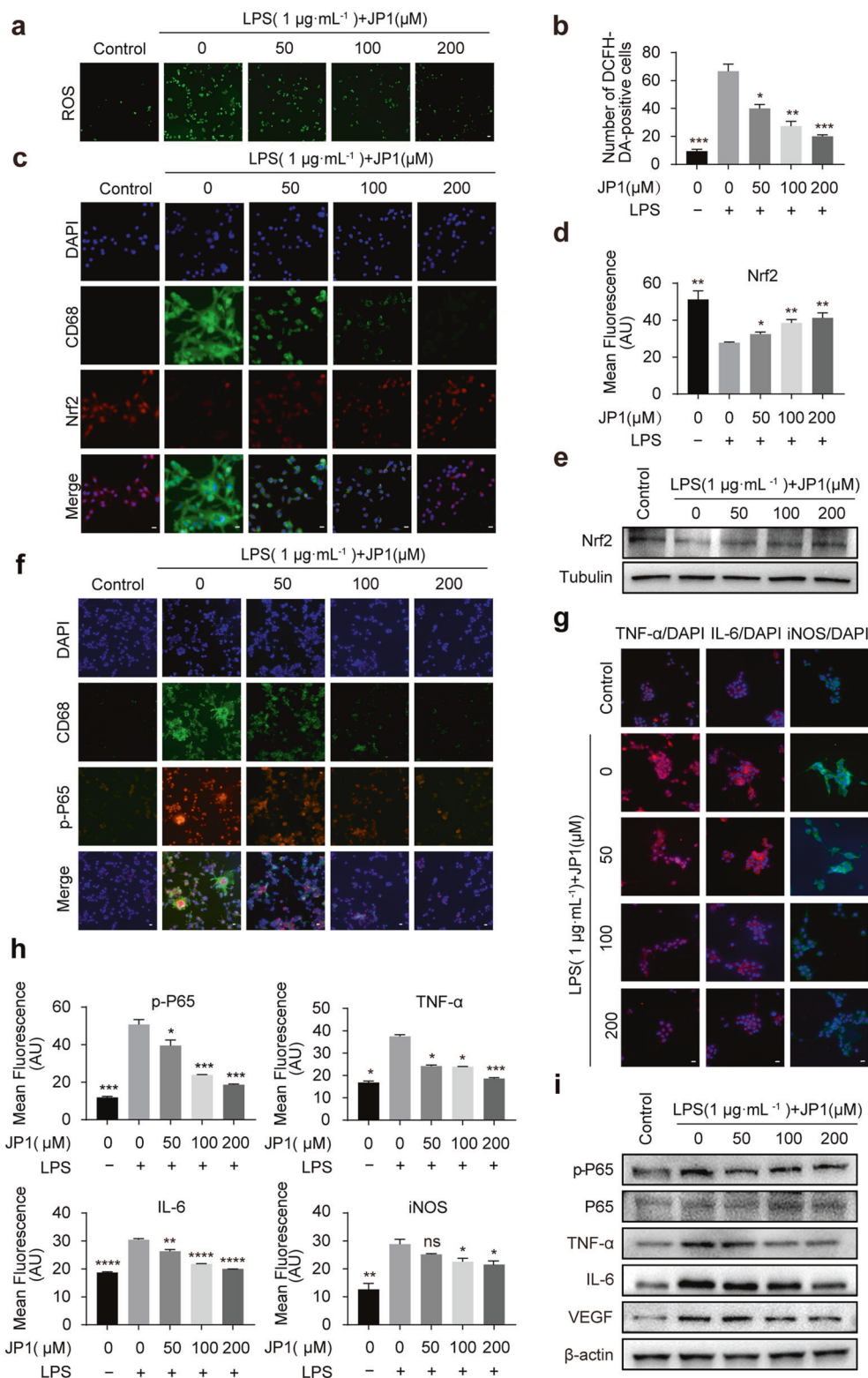
Fig. 4 JP1 suppressed LPS-induced oxidative stress and inflammation in BV2 cells. a Intracellular ROS levels measured using DCFH-DA in LPS-stimulated BV2 cells in the presence or absence of JP1, scale bar: 20 μm. **b** Measurement of DCFH-DA-positive cells by confocal microscopy. **c** Immunofluorescent evaluation of Nrf2 and CD68 in BV2 cells, scale bar: 20 μm. **d** Mean fluorescence of Nrf2 in BV2 cells. **e** Western blot analysis of Nrf2 in BV2 cells. **f** Immunofluorescent evaluation of p-P65 and CD68 in BV2 cells, scale bar: 20 μm. **g** Immunofluorescent evaluation of TNF-α, IL-6 and iNOS in BV2 cells, scale bar: 20 μm. **h** Quantitative analysis of the mean fluorescence of p-P65, TNF-α, IL-6, and iNOS in BV2 cells. **i** Western blot analysis of p-P65, P65, VEGF, TNF-α and IL-6 in BV2 cells. Data in **b**, **d**, and **h** were expressed mean ± SEM. ns no difference from group treated with LPS (1 μg·mL^{-1}); *$P \leq 0.05$ vs group treated with LPS (1 μg·mL^{-1}); **$P \leq 0.01$ vs group treated with LPS (1 μg·mL^{-1}); ***$P \leq 0.001$ vs group treated with LPS (1 μg·mL^{-1}); ****$P \leq 0.0001$ vs group treated with LPS (1 μg·mL^{-1}). NT non-treated.
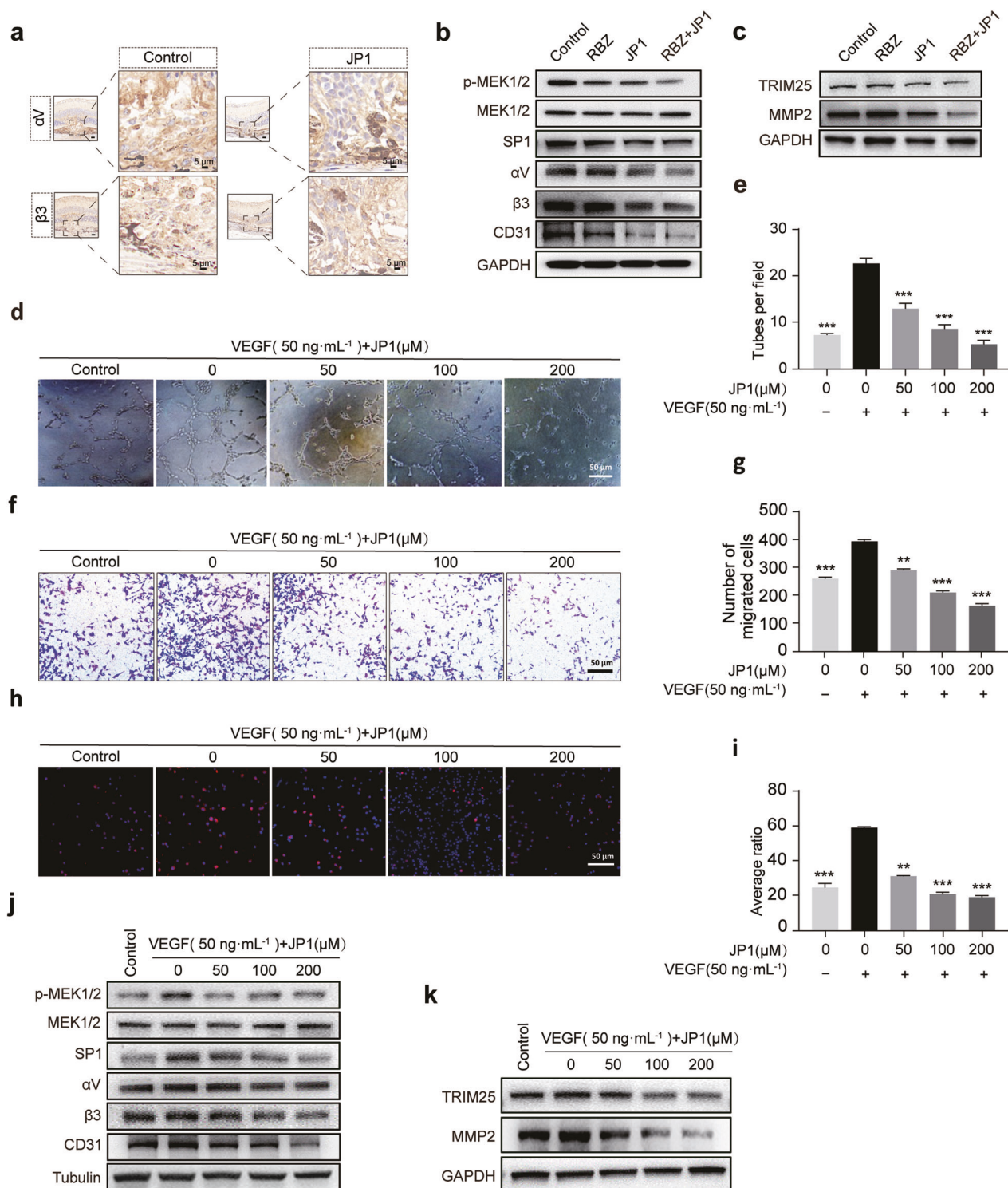
Fig. 5 JP1 inhibited angiogenesis through regulating the MEK1/2-SP1-Integrin αVβ3 and TRIM25-SP1-MMP2 axes both in vivo and in vitro. a Immunohistochemical staining showed the expression of integrin αV and β3 in choroidal neovascular tissue of CNV lesions. Images on the right of each pair showed an enlarged view of the areas framed in the small image, scale bar in the small image: 20 μm, scale bar in the large image: 5 μm. **b** Western blot analysis of the protein levels of p-MEK1/2, MEK1/2, SP1, integrin αV, β3 and CD31 in the choroid-scleral complex in IVT injection groups treated with 1 μL of PBS, 10 μg of ranibizumab, 40 μg of JP1 and combined treatment (5 μg of ranibizumab + 20 μg of JP1). **c** Western blot analysis of TRIM25 and MMP2 in the choroid-scleral complex in IVT injection groups. **d–i** JP1 inhibited the tube formation, migration and proliferation of HUVECs in vitro. HUVECs were treated with VEGF (50 ng mL^{-1}) in the presence or absence of JP1 at indicated doses (0, 50, 100, 200 μM) for 24 h. Tube formation assay was performed (**d**) and closed tubes were counted (**e**) Transwell assay (**f**) was performed to detect the migrative capability of HUVECs and migrated cells were counted (**g**). EdU assay (**h**) was performed to measure the proliferative capability of HUVECs and the EdU-positive cell ratio (**i**). **j, k** Western blot analysis of the protein levels of p-MEK1/2, MEK1/2, SP1, integrin αV, β3, CD31, TRIM25 and MMP2 of HUVECs treated with VEGF (50 ng· mL^{-1}) in the presence or absence of JP1. Data in **e–g**, and **i** were expressed as mean ± SEM. **$P \le 0.01$ vs group treated with VEGF (50 ng· mL^{-1}), ***$P \le 0.001$ vs group treated with VEGF (50 ng· mL^{-1}).
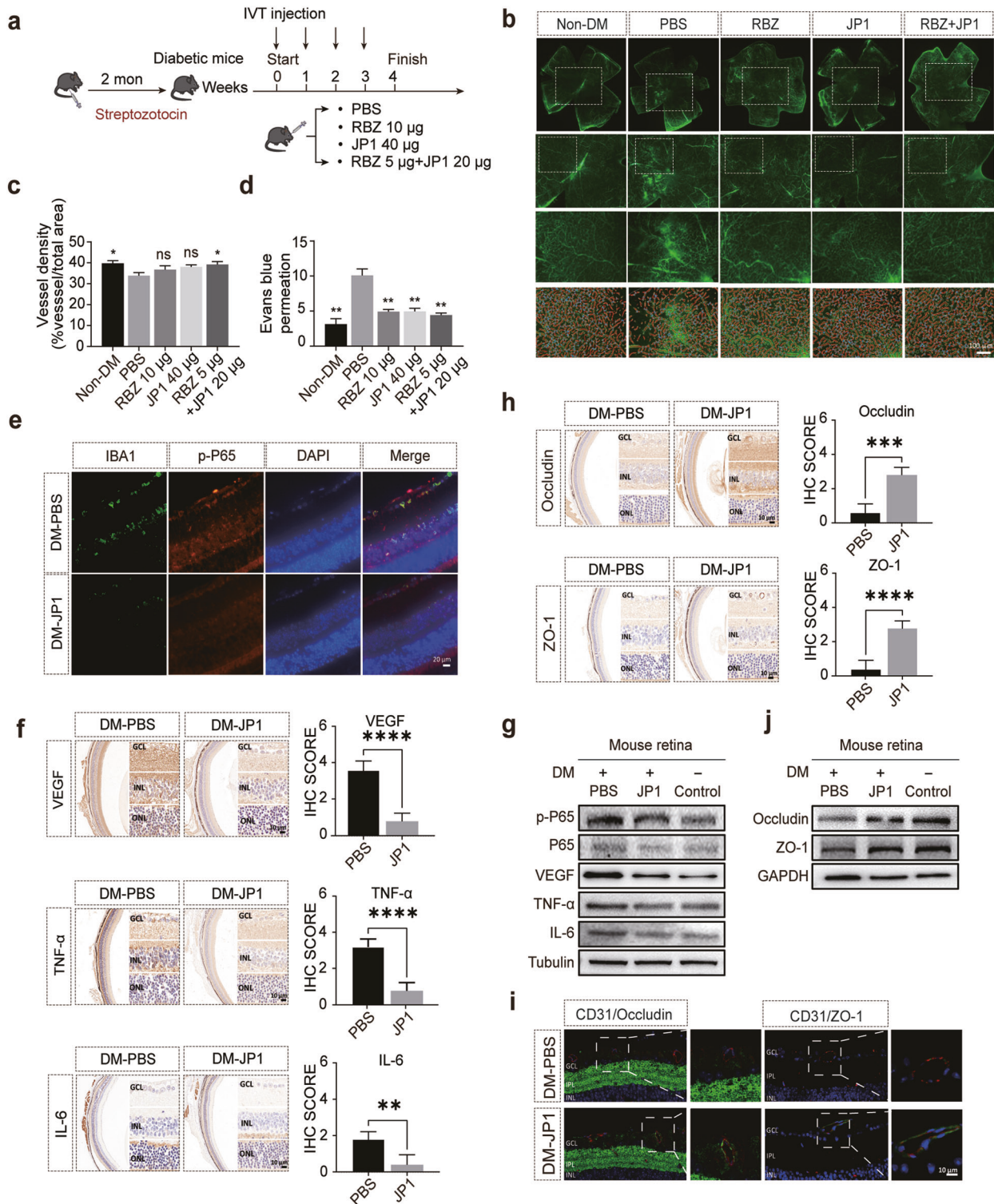
Fig. 6 JP1 inhibited vascular leakage in the mouse STZ model. a Schematic diagram of experimental procedures. **b** Fluorescence micrographs of fluorescein-dextran-perfused retinae in flat mounts. Low and high-magnification fluorescein angiographs of retinal whole mounts obtained from control, RBZ, JP1 and combined groups at 3 Mon after STZ-injection, scale bar: 100 μm. **c** Quantitative analysis of vascular density in each eye evaluated by AngioTool. **d** Quantitative analysis of Evans blue leakage in all groups ($n = 3$ mice per group). **e** Immunofluorescence analysis of IBA1 and p-P65 in the retinal tissue from diabetic mice treated with PBS and JP1, scale bar: 20 μm. **f** Immunohistochemical analysis of TNF-α, IL-6 and VEGF in the retinal tissues from diabetic mice treated with PBS and JP1, scale bar: 10 μm. **g** Western blot analysis of the protein levels of p-P65, P65, VEGF, TNF-α and IL-6 in diabetic mouse retinae treated with PBS and JP1. **h** Immunohistochemical analysis of Occludin and ZO-1 in the retinal tissue from diabetic mice treated with PBS and JP1. **i** Immunofluorescence images showing the expression of CD31, Occludin, and ZO-1 in the nerve fiber and ganglion cell layer in the retinal tissue from diabetic mice treated with PBS and JP1, scale bar: 10 μm. **j** Western blot analysis of Occludin and ZO-1 in the retinae of diabetic mice treated with PBS and JP1. Data in **c**, **d**, **f**, and **h** were expressed as mean ± SEM. *$P \leq 0.05$ vs PBS group, **$P \leq 0.01$ vs PBS group, ***$P \leq 0.001$ vs PBS group, ****$P \leq 0.0001$ vs PBS group.

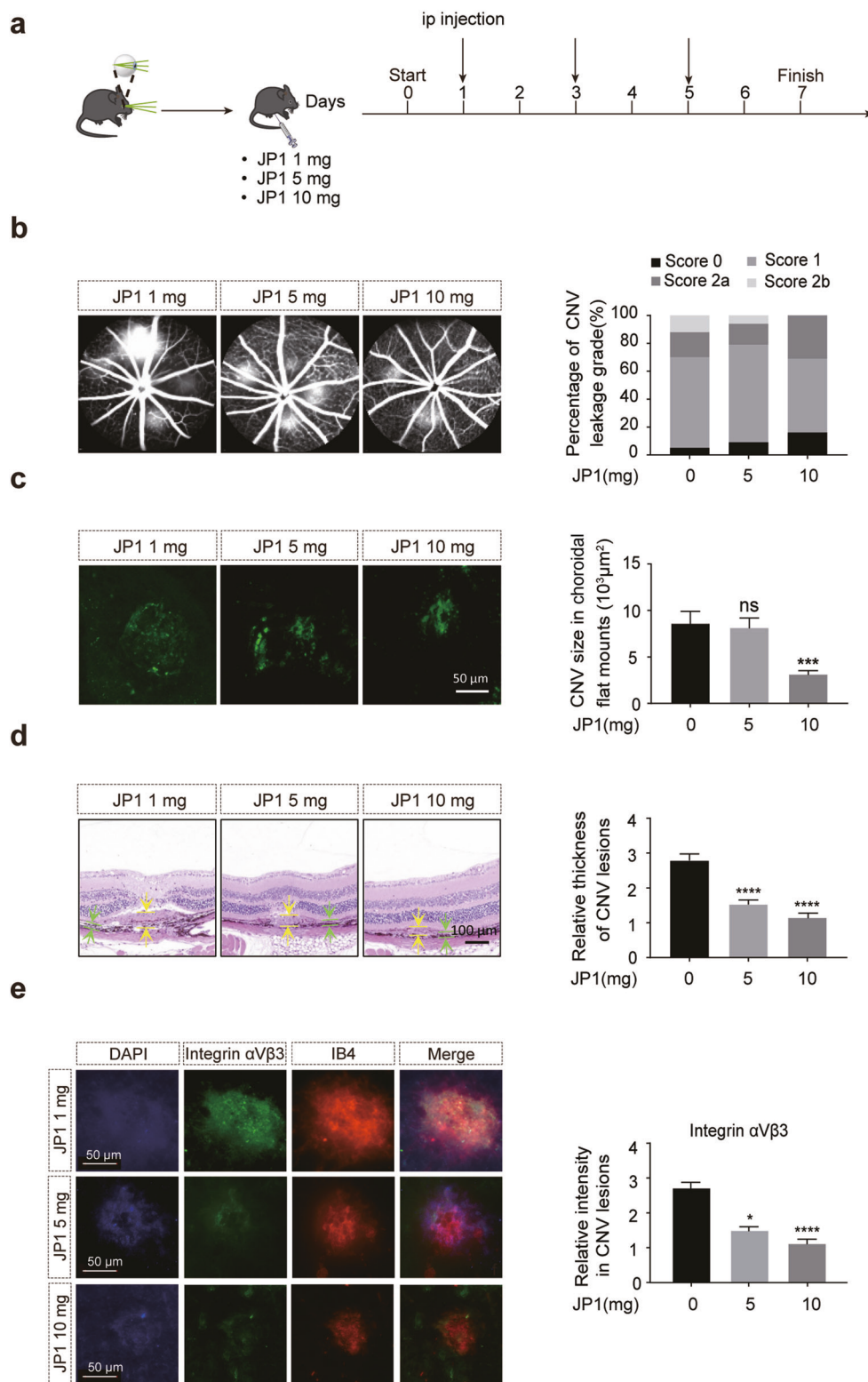**Fig. 7 Intraperitoneal injection of JP1 reduces CNV leakage and area. a** Schematic diagram of the experimental procedure of CNV mouse models intraperitoneally injected with JP1. **b** Representative FFA images of CNV lesions leakage and quantitative analysis of CNV lesions leakage in mice intraperitoneally injected with JP1. **c** Typical images of FITC-dextran-labeled blood vessels on a flat-mounted choroid and quantification of the area with fluorescent vessels by ImageJ software, scale bar: 50 μm. **d** HE staining of CNV lesions and quantitative analysis of relative CNV lesion thickness, scale bar: 100 μm. **e** Immunofluorescent evaluation of integrin αVβ3 (green) and IB4 (red) in choroidal neovascular tissue of CNV lesions and quantitative analysis of the mean intensity of integrin αVβ3 in CNV lesions, scale bar: 50 μm. Data in **b**, **c**, **d**, and **e** were expressed as mean ± SEM. Ns, for no difference from JP1(1 mg, i.p.) group, *$P \leq 0.05$ vs JP1(1 mg, i.p.) group, ***$P \leq 0.001$ vs JP1(1 mg, i.p.) group, ****$P \leq 0.0001$ vs JP1(1 mg, i.p.) group.
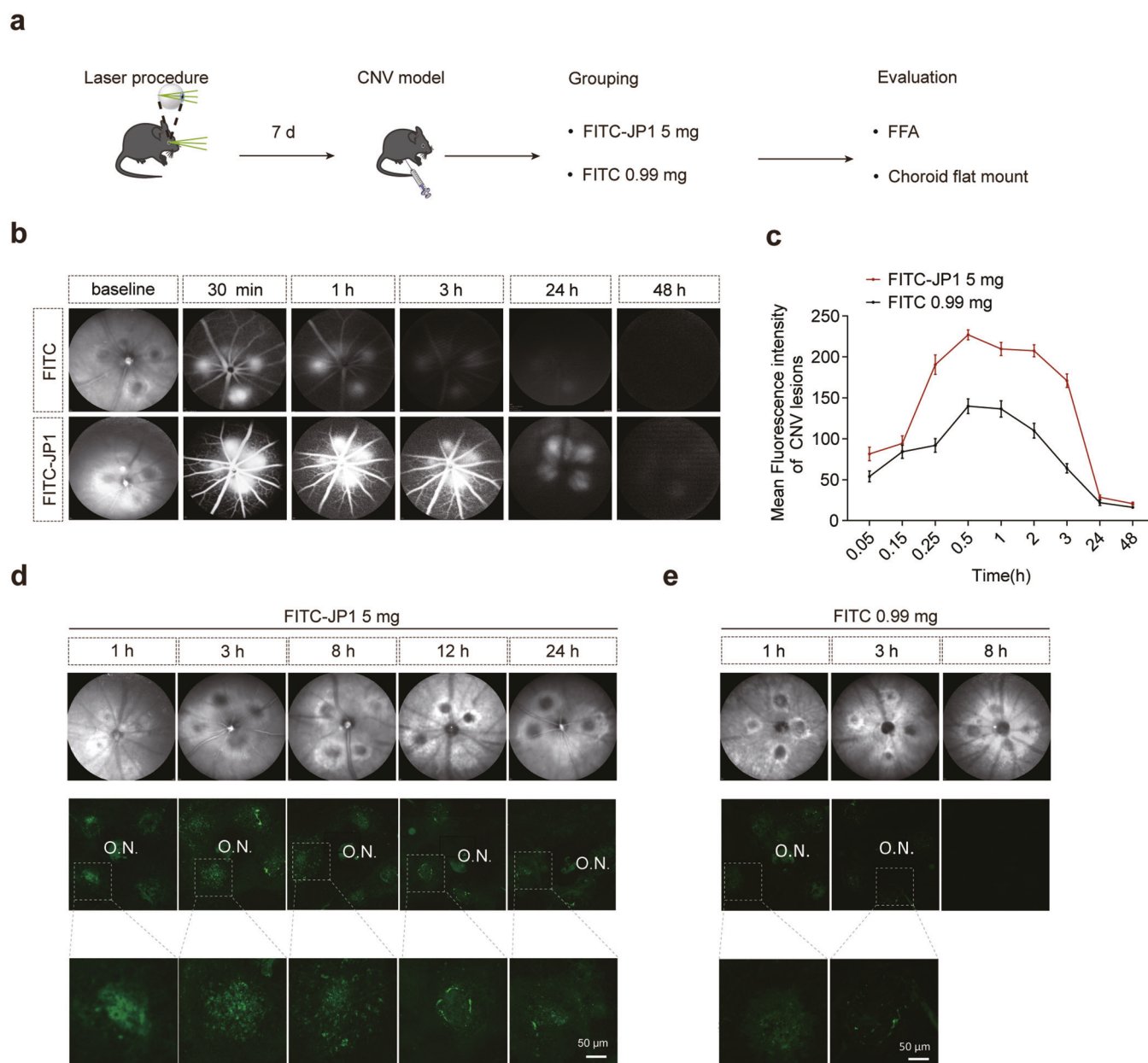
a

b

c

d

e

Fig. 8   JP1 i.p. treatment enhances FITC accumulation in the CNV area. a Schematic diagram of experimental procedures in the CNV mouse model intraperitoneally injected with FITC-JP1 and FITC; Representative FFA images (**b**) and quantitative analysis (**c**) of CNV lesion fluorescence intensity in FITC-JP1 and FITC group. **d**, **e** Representative fluorescent images of flat-mounted choroid at indicated time points after i.p. injection in two groups (FITC-JP1 5 mg vs FITC 0.99 mg), scale bar: 50 μm. Data in **c** were expressed as mean ± SEM. O.N. optic nerve.

findings may refresh current understanding about the mechanism of CNV and treatment options for nAMD and DR.

Anti-VEGF therapies have harvested inspiring outcomes in the treatment of nAMD and DME, but its widely use is still restricted by burden from frequent IVT injections. Researchers have identified that in the treatment of nAMD, resistance to an anti-VEGF therapy may arise from mechanisms unrelated to VEGF [53]. In this study, we found that JP1 suppressed CNV via "multiple targets" in the laser-induced mouse model (Fig. 9), rendering it capabilities to overcome patients' resistance to traditional anti-VEGF therapy.

Substantial evidence suggests that microglial cells rely on their complex immune checkpoints and plasticity to control retinal homeostasis [45]. In some cases, however, inflammation may not subside due to positive feedback mechanisms of pro-inflammatory components triggered by persistent tissue stress

and deleterious signals [54]. In this state, the immune checkpoints of microglia become counterproductive and their ability to restrain inflammation is blocked [55]. The excessive release of pro-inflammatory molecules by microglia can worsen the disease. Therefore, the next-generation of therapeutic strategy should focus on the modulation of microglial reactivity [56]. In this study, we detected that JP1 decreased the recruitment and activation of microglial cells in CNV lesions at d 7 after laser treatment (Fig. 2a, b). Chemokines CCL2, CCL22, CXCL10, IL-6, IL-8 and IL-10 were all significantly downregulated in the JP1-treated RPE/choroids (Fig. 2c, h). Both in vivo and in vitro experiments showed JP1 counteracted oxidative stress and inflammation via inhibiting the ROS/NF-κB signaling in microglial cells (Figs. 3 and 4). JWA gene has been reported to alleviate oxidative stress and inhibit inflammation in the neurotoxin mouse model of Parkinson's
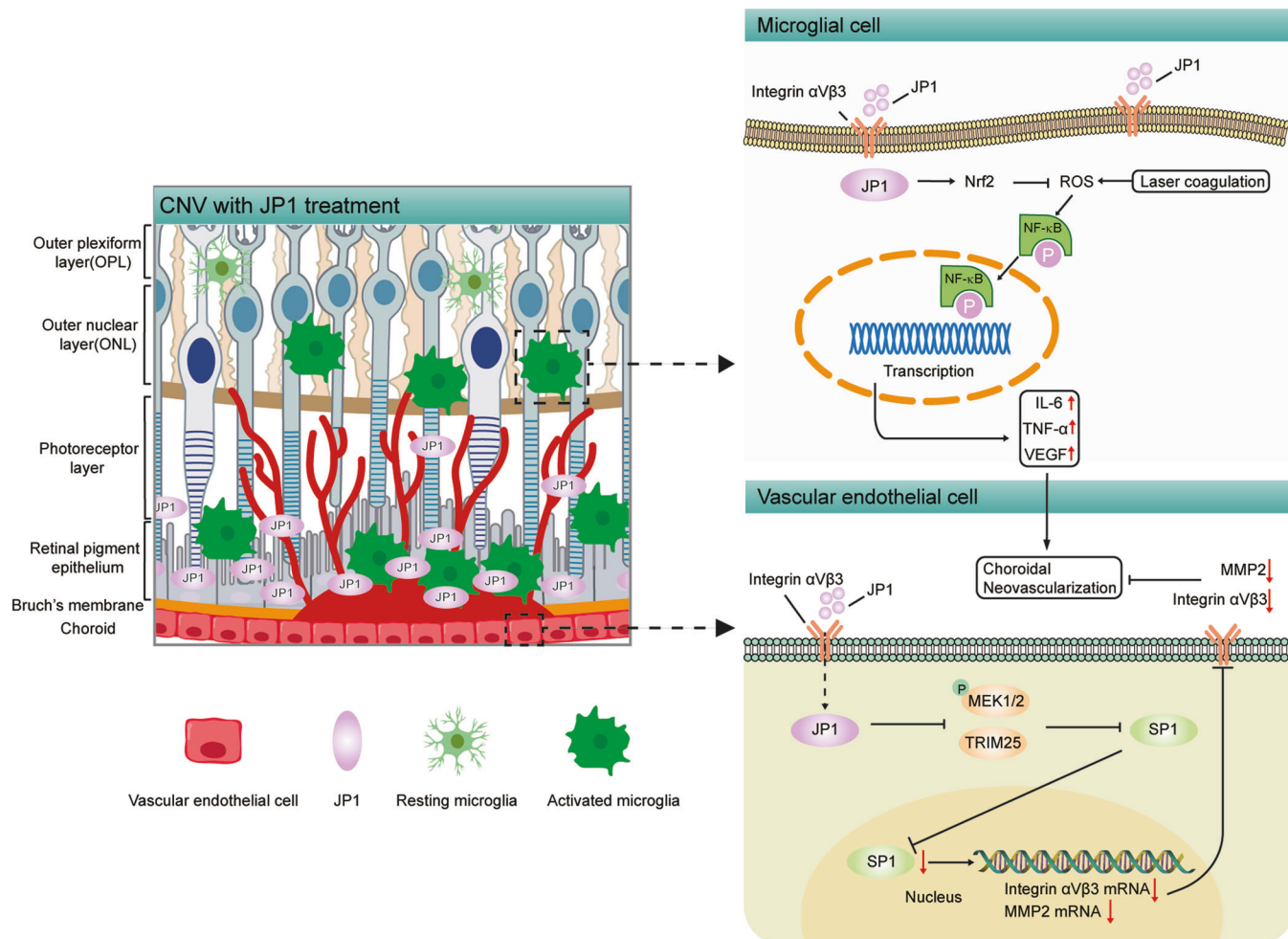
Fig. 9 Graphical summary of finding. Our findings verified the therapeutic efficacy of JP1 on laser-induced CNV and STZ-induced diabetes in the mouse models. The underlying mechanism is dichotomous. On one hand, JP1 counteracts oxidative stress and inflammation via repressing the NF-κB pathway in microglial cells. On the other hand, JP1 plays antiangiogenic role via inhibiting the phosphorylation of MEK1/2 and TRIM25, accelerating the degradation of SP1, and hindering the transcription of integrin αVβ3 and MMP2 in vascular endothelial cells.

disease [57]. JWA antagonizes paraquat-induced neurotoxicity via activating Nrf2 and reducing ROS [34]. In addition, JWA gene protects against dopaminergic neuronal degeneration via modulating intracellular redox status and the NF-κB signaling pathway [50]. Our findings are consistent with those reported in literatures [34, 50, 57].

As oxidative stress, inflammation and neovascularization are three pathological events intimately implicated in AMD [58], we explored the effect and mechanism of JP1 in inhibiting angiogenesis with in vivo and in vitro experiments. We found that JP1 modulated MEK1/2/SP1/Integrin αVβ3 and TRIM25/SP1/MMP2 axes in vascular endothelial cells, which suppressed the neovascular growth in the mouse model of CNV (Fig. 5). Our findings confirmed the hypothesis that JP1 inhibits CNV through a mechanism similar to that of JWA in countering tumorigenesis [21, 38, 39]. Moreover, we discovered that IVT injection of JP1 with anti-VEGF antibody was superior to that of anti-VEGF antibody alone in attenuating angiogenesis, indicating that the combination arouses different therapeutic mechanisms for CNV (Fig. 1b–g). These data suggest that JP1 may be exploited to design novel options for patients who show incomplete responses to traditional anti-VEGF therapies.

We also confirmed that extraocular injection of JP1 (by i.p. injection) effectively inhibited laser-induced CNV in a dose-dependent manner (Fig. 7). Currently, most of drugs for posterior

ocular neovascularization are delivered through IVT injection. It is an invasive route, but alternative clinical outcomes are bleak at present [59–61]. Two basic approaches are expected to improve the therapeutic outcomes: prolonging delivery of intravitreal drugs and using other routes [61]. Topical eye drops are convenient and non-invasive, but less effective, because the corneal, conjunctival epithelia, and tear film together prop up a barrier that blocks the penetration of eye drops, as shown by their low bioavailability and concentration in the posterior eye [62]. Therefore, we can expect to create drugs based on JP1 (i.p.) that may break through ocular barriers to target CNV.

Integrin αVβ3, a main RGD integrin engaged in the development of nAMD and DR, is overexpressed in new ocular blood vessels under a pathological condition [14, 63]. Thus, integrin αvβ3 may be targeted to deliver ocular drugs to the CNV lesion [63]. JP1 is an RGD-modified peptide specifically binding to integrin αVβ3. In this study, double staining of Integrin αVβ3 and IB4 on choroidal flat mounts showed significant downregulation in JP1 i.p. groups dose-dependently at d 7 after laser induction (Fig. 7e). Analytic results about FFA and choroidal flat mounts confirmed the efficacy of JP1 (i.p.) on CNV (Fig. 7a–d). Furthermore, fluorescence intensity in eyes increased in the FITC-JP1 group, according to that in the FITC group in the CNV mouse model, indicating that JP1 (i.p.) enhances FITC accumulation in the CNV area (Fig. 8). These data suggest that JP1 can penetrate the BRB to

target CNV lesion, thus significantly improved the drug concentration within the diseased tissue.

Notably, systemic medication may bring with extensive side effects and possible toxicity. However, JP1, a functional polypeptide derived from the active fragment of human JWA protein, demonstrates no immunogenicity in mouse due to its high homology. After iv injection of JP1 (either 45 or 150 mg·kg^{-1} per day for 14 d), cynomolgus monkeys exhibit no significant differences in a file of parameters, including clinical symptoms, weight, food take, body temperature, ophthalmology, electrocardiogram, blood routine examination, blood biochemistry, blood coagulation, urinalysis and immune-toxicity [21]. In the present study, we did not observe any damage or toxicity to mouse eyes, suggesting that JP1 might be preferable for patients with low compliance and intraocular complications associated with repeated IVT injections.

Limitations also exist in this study. First, only mice with laser-induced CNV and STZ-induced diabetes were used in this study. Though they have been proved valuable in drug screening [64], a primate model is needed to validate our findings. Second, genomic mutations in vascular endothelial cells may lead to conformational changes in receptors and affect the sensitivity to antiangiogenic agents [5, 53]. In heterogeneous endothelial cells, JP1 may not target integrin αVβ3. Therefore, exploring other targets of JP1 is a research objective in the future.

CONCLUSION
Intraocular injection of JP1 suppressed CNV in the laser-induced mouse model and vascular leakage in the streptozotocin-induced diabetic mouse model. JP1 i.p. treatment potently inhibited CNV in a dose-dependent manner. Mechanistically, JP1 might relieve CNV via repressing the ROS/NF-κB signaling pathway in microglial cells and modulating the MEK1/2-SP1-Integrin αVβ3 and TRIM25-SP1-MMP2 axes in vascular endothelial cells. JP1 provided a new therapeutic idea for neovascular ocular diseases, especially for patients who are clinically insensitive to anti-VEGF drugs or require repeated injections that may cause serious side effects.

AUTHOR CONTRIBUTIONS
ZX, STY, JWZ, and QHL designed the research project; ZX, XJW, RWC, and JHC performed the research; ZX, JHC, STY, JWZ, and QHL analyzed the data; ZX wrote the manuscript draft; ZX, STY, JWZ and QHL revised the manuscript.

ADDITIONAL INFORMATION
Competing interests: The authors declare no competing interests.

REFERENCES
1. Yun JH. Hepatocyte growth factor prevents pericyte loss in diabetic retinopathy. Microvasc Res. 2021;133:104103.
2. Granstam E, Aurell S, Sjövall K, Paul A. Switching anti-VEGF agent for wet AMD: evaluation of impact on visual acuity, treatment frequency and retinal morphology in a real-world clinical setting. Graefes Arch Clin Exp Ophthalmol. 2021;259:2085–93.
3. Cécile D. Epidemiology of age-related macular degeneration. La Rev du praticien. 2017;67:88–91.
4. Mettu PS, Allingham MJ, Cousins SW. Incomplete response to anti-VEGF therapy in neovascular AMD: Exploring disease mechanisms and therapeutic opportunities. Prog Retin Eye Res. 2020;82:100906.
5. Sun X, Yang S, Zhao J. Resistance to anti-VEGF therapy in neovascular age-related macular degeneration: a comprehensive review. Drug Des Dev Ther. 2016;10:1857–67.
6. Ehlken C, Jungmann S, Bhringer D, Agostini HT, Pielen A. Switch of anti-VEGF is an option for nonresponders in the treatment of AMD. Eye. 2014;28:538–45.
7. Tian Y, Zhang F, Qiu Y, Wang S, Li F, Zhao J, et al. Reduction of choroidal neovascularization via cleavable VEGF antibodies conjugated to exosomes derived from regulatory T cells. Nat Biomed Eng. 2021;5:968–82.
8. Wallsh JO, Gallemore RP. Anti-VEGF-resistant retinal diseases: a review of the latest treatment options. Cells. 2021;10:1049.
9. Pb A, Nam A, Tacma B, Wudunn AD, Lbc A. The acute and chronic effects of intravitreal anti-vascular endothelial growth factor injections on intraocular pressure: a review. Surv Ophthalmol. 2018;63:281–95.
10. Baek SU, Park IW, Suh W. Long-term intraocular pressure changes after intravitreal injection of bevacizumab. Cutan Ocul Toxicol. 2016;35:310–4.
11. Rayess N, Rahimy E, Storey P, Shah CP, Wolfe JD, Chen E, et al. Postinjection endophthalmitis rates and characteristics following intravitreal bevacizumab, ranibizumab, and aflibercept. Am J Ophthalmol. 2016;165:88–93.
12. Ren C, Hui S, Jiang J, Liu Q, Du Y, He M, et al. The effect of CM082, an oral tyrosine kinase inhibitor, on experimental choroidal neovascularization in rats. J Ophthalmol. 2017;2017:6145651.
13. Kechagia JZ, Ivaska J, Roca-Cusachs P. Integrins as biomechanical sensors of the microenvironment. Nat Rev Mol Cell Biol. 2019;20:1–17.
14. Hu TT, Vanhove M, Porcu M, Van Hove I, Van Bergen T, Jonckx B, et al. The potent small molecule integrin antagonist THR-687 is a promising next-generation therapy for retinal vascular disorders. Exp Eye Res. 2019;180:43–52.
15. Umeda N, Shu K, Akiyama H, Zahn G, Campochiaro PA. Suppression and regression of choroidal neovascularization by systemic administration of an α5β1 integrin antagonist. Mol Pharmacol. 2006;69:1820–8.
16. Ramakrishnan V, Bhaskar V, Law DA, Wong MH, DuBridge RB, Breinberg D, et al. Preclinical evaluation of an anti-alpha5beta1 integrin antibody as a novel anti-angiogenic agent. J Exp Ther Oncol. 2006;5:273–86.
17. Nebbioso M, Lambiase A, Cerini A, Limoli PG, La Cava M, Greco A. Therapeutic approaches with intravitreal injections in geographic atrophy secondary to age-related macular degeneration: current drugs and potential molecules. Int J Mol Sci. 2019;20:1693.
18. Askew BC, Furuya T, Edwards DS. Pharmacodynamics and pharmacokinetics of SF0166, a topically administered αvβ3 integrin antagonist, for the treatment of retinal diseases. J Pharmacol Exp Ther. 2018;366:jpet.118.248427.
19. Cao H, Xia W, Shen Q, Hua L, Jian Y, Li A, et al. Role of JWA in acute promyelocytic leukemia cell differentiation and apoptosis triggered by retinoic acid, 12-tetradecanoylphorbol-13-acetate and arsenic trioxide. Chin Sci Bull. 2002;47:834–8.
20. Chen Y, Huang Y, Huang Y, Xia X, Zhang J, Zhou Y, et al. JWA suppresses tumor angiogenesis via Sp1-activated matrix metalloproteinase-2 and its prognostic significance in human gastric cancer. Carcinogenesis. 2014;35:442–51.
21. Cui J, Shu C, Xu J, Chen D, Zhou J. JP1 suppresses proliferation and metastasis of melanoma through MEK1/2 mediated NEDD4L-SP1-Integrin αvβ3 signaling. Theranostics. 2020;10:8036–50.
22. Lambert V, Lecomte J, Hansen S, Blacher S, Gonzalez M, Struman I, et al. Laser-induced choroidal neovascularization model to study age-related macular degeneration in mice. Nat Protoc. 2013;8:2197–211.
23. Li L, Zhu M, Wu W, Qin B, Ding D. Brivanib, a multitargeted small-molecule tyrosine kinase inhibitor, suppresses laser-induced CNV in a mouse model of neovascular AMD. J Cell Physiol. 2020;235:1259–73.
24. Lai K, Gong Y, Zhao W, Li L, Jin C. Triptolide attenuates laser-induced choroidal neovascularization via M2 macrophage in a mouse model. Biomed Pharmacother. 2020;129:110312.
25. Bergen TV, Hu TT, Etienne I, Reyns GE, Moons L, Feyen J Neutralization of placental growth factor as a novel treatment option in diabetic retinopathy. Exp Eye Res. 2017:S0014483517304505.
26. Naderi A, Zahed R, Aghajanpour L, Amoli FA, Lashay A. Long term features of diabetic retinopathy in streptozotocin-induced diabetic Wistar rats. Exp Eye Res. 2019;184:213–20.
27. Indaram M, Ma W, Zhao L, Fariss RN, Rodriguez IR, Wong WT. 7-Ketocholesterol increases retinal microglial migration, activation, and angiogenicity: a potential pathogenic mechanism underlying age-related macular degeneration. Sci Rep. 2015;5:9144.
28. Karlstetter M, Scholz R, Rutar M, Wong WT, Provis JM, Langmann T. Retinal microglia: just bystander or target for therapy? Prog Retin Eye Res. 2015;45:30–57.
29. Kinuthia UM, Wolf A, Langmann T. Microglia and inflammatory responses in diabetic retinopathy. Front Immunol. 2020;11:564077.
30. Yang Y, Liu F, Tang M, Yuan M, Hu A, Zhan Z, et al. Macrophage polarization in experimental and clinical choroidal neovascularization. Sci Rep. 2016;6:30933.

912

31. Bretz CA, Divoky V, Prchal J, Kunz E, Simmons AB, Wang H, et al. Erythropoietin signaling increases choroidal macrophages and cytokine expression, and exacerbates choroidal neovascularization. Sci Rep. 2018;8:2161.

32. Yeo NJY, Chan EJJ, Cheung C. Choroidal neovascularization: mechanisms of endothelial dysfunction. Front Pharmacol. 2019;10:1363.

33. Kim SY, Kambhampati SP, Bhutto IA, Mcleod DS, Kannan RM. Evolution of oxidative stress, inflammation and neovascularization in the choroid and retina in a subretinal lipid induced age-related macular degeneration model. Exp Eye Res. 2020;203:108391.

34. Zhao X, Wang R, Xiong J, Yan D, Li A, Wang S, et al. JWA antagonizes paraquat-induced neurotoxicity via activation of Nrf2. Toxicol Lett. 2017;277:32–40.

35. Datta S, Cano M, Ebrahimi K, Wang L, Handa JT. The impact of oxidative stress and inflammation on RPE degeneration in non-neovascular AMD. Prog Retin Eye Res. 2017;60:201–18.

36. Lier J, Streit WJ, Bechmann I. Beyond activation: characterizing microglial functional phenotypes. Cells. 2021;10:2236.

37. Kim YJ, Park SY, Koh YJ, Lee JH. Anti-neuroinflammatory effects and mechanism of action of Fructus ligustri lucidi extract in BV2 microglia. Plants. 2021;10:688.

38. Lu J, Tang Y, Farshidpour M, Cheng Y, Zhang G, Jafarnejad SM, et al. JWA inhibits melanoma angiogenesis by suppressing ILK signaling and is an independent prognostic biomarker for melanoma. Carcinogenesis. 2013;34:2778–88.

39. Chen JJ, Ren YL, Shu CJ, Zhang Y, Chen MJ, Xu J, et al. JP3, an antiangiogenic peptide, inhibits growth and metastasis of gastric cancer through TRIM25/SP1/MMP2 axis. J Exp Clin Cancer Res. 2020;39:118.

40. Capitão M, Soares R. Angiogenesis and inflammation crosstalk in diabetic retinopathy. J Cell Biochem. 2016;117:2443–53.

41. Hamdan F, Bigdeli Z, Asghari SM, Sadremomtaz A, Balalaie S. Synthesis of modified RGD-based peptides and their in vitro activity. ChemMedChem. 2019;14:282–8.

42. Semeraro F, Cancarini A, Dell'Omo R, Rezzola S, Romano MR, Costagliola C. Diabetic retinopathy: vascular and inflammatory disease. J Diabetes Res. 2015;2015:1–16.

43. Arroba AI, Valverde Á. Modulation of microglia in the retina: new insights into diabetic retinopathy. Acta Diabetol. 2017;54:527.

44. Wang M, Wang X, Zhao L, Ma W, Rodriguez IR, Fariss RN, et al. Macroglia-microglia interactions via TSPO signaling regulates microglial activation in the mouse retina. J Neurosci. 2014;34:3793–806.

45. Alves CH, Fernandes R, Santiago AR, Ambrósio AF. Microglia contribution to the regulation of the retinal and choroidal vasculature in age-related macular degeneration. Cells. 2020;9:1217.

46. Zhang T, Ouyang H, Mei X, Lu B, Yu Z, Chen K, et al. Erianin alleviates diabetic retinopathy by reducing retinal inflammation initiated by microglial cells via inhibiting hyperglycemia-mediated ERK1/2-NF-κB signaling pathway. FASEB J. 2019;33:11776–90.

47. Chen N, Jiang K, Yan GG. Effect of fenofibrate on diabetic retinopathy in rats via SIRT1/NF-κB signaling pathway. Eur Rev Med Pharmacol Sci. 2019;23:8630–6.

48. Cai Y, Li W, Tu H, Chen N, Zhong Z, Yan P, et al. Curcumolide reduces diabetic retinal vascular leukostasis and leakage partly via inhibition of the p38MAPK/NF-κB signaling. Bioorg Med Chem Lett. 2017;27:1835–9.

49. Popiolek-Barczyk K, Mika J. Targeting the microglial signaling pathways: new insights in the modulation of neuropathic pain. Curr Med Chem. 2016;23:2908–28.

50. Miao SH, Sun HB, Ye Y, Yang JJ, Shi YW, Lu M, et al. Astrocytic JWA expression is essential to dopaminergic neuron survival in the pathogenesis of Parkinson's disease. CNS Neurosci Ther. 2014;20:754–62.

51. Bhatwadekar AD, Kansara V, Luo Q, Ciulla T. Anti-integrin therapy for retinovascular diseases. Expert Opin Investig Drugs. 2020;29:935–45.

52. Sani S, Messe M, Fuchs Q, Pierrevelcin M, Laquerriere P, Entz-Werle N, et al. Biological relevance of RGD-integrin subtype-specific ligands in cancer. Chembiochem. 2021;22:1151–60.

53. Mettu PS, Allingham MJ, Cousins SW. Incomplete response to Anti-VEGF therapy in neovascular AMD: Exploring disease mechanisms and therapeutic opportunities. Prog Retin Eye Res. 2021;82:100906.

54. Sheets KG, Jun B, Zhou Y, Zhu M, Petasis NA, Gordon WC, et al. Microglial ramification and redistribution concomitant with the attenuation of choroidal neovascularization by neuroprotectin D1. Mol Vis. 2013;19:1747–59.

55. Deczkowska A, Amit I, Schwartz M. Microglial immune checkpoint mechanisms. Nat Neurosci. 2018;21:779–86.

56. Hikage F, Lennikov A, Mukwaya A, Lachota M, Ida Y, Utheim TP, et al. NF-κB activation in retinal microglia is involved in the inflammatory and neovascularization signaling in laser-induced choroidal neovascularization in mice. Exp Cell Res. 2021;403:112581.

57. Wang R, Zhao X, Xu J, Wen Y, Li A, Lu M, et al. Astrocytic JWA deletion exacerbates dopaminergic neurodegeneration by decreasing glutamate transporters in mice. Cell Death Dis. 2018;9:352.

58. Kim SY, Kambhampati SP, Bhutto IA, McLeod DS, Lutty GA, Kannan RM. Evolution of oxidative stress, inflammation and neovascularization in the choroid and retina in a subretinal lipid induced age-related macular degeneration model. Exp Eye Res. 2021;203:108391.

59. Bulbake U, Doppalapudi S, Kommineni N, Khan W. Liposomal formulations in clinical use: an updated review. Pharmaceutics. 2017;9:12.

60. Chu Y, Chen N, Yu H, Mu H, He B, Hua H, et al. Topical ocular delivery to laser-induced choroidal neovascularization by dual internalizing RGD and TAT peptide-modified nanoparticles. Int J Nanomed. 2017;12:1353–68.

61. Del Amo EM, Rimpelä AK, Heikkinen E, Kari OK, Ramsay E, Lajunen T, et al. Pharmacokinetic aspects of retinal drug delivery. Prog Retin Eye Res. 2017;57:134–85.

62. Gote V, Sikder S, Sicotte J, Pal D. Ocular drug delivery: present innovations and future challenges. J Pharmacol Exp Ther. 2019;370:602–24.

63. Cai W, Chen Q, Shen T, Yang Q, Hu W, Zhao P, et al. Intravenous anti-VEGF agents with RGD peptide-targeted core cross-linked star (CCS) polymers modified with indocyanine green for imaging and treatment of laser-induced choroidal neovascularization. Biomater Sci. 2020;8:4481–91.

64. Wang X, Lou N, Eberhardt A, Yang Y, Kusk P, Xu Q, et al. An ocular glymphatic clearance system removes β-amyloid from the rodent eye. Sci Transl Med. 2020;12:eaaw3210.